Acta Geochim (2024) 43:72–86
https://doi.org/10.1007/s11631-023-00644-4

ORIGINAL ARTICLE

Petrogenesis and tectonic implications of the Silurian adakitic granitoids in the eastern segment of the Qilian Orogenic Belt, Northwest China

Jiao-Long Zhao[1] · Xiao-Jun Huang[2] · Pei-Qing Hu[1] · Zhen-Xi Yang[3] · Ying Fan[3] · Er-Teng Wang[1] · Fu-Bo Yang[1] · Jing-Yu Zhang[1]

Received: 12 August 2023 / Revised: 6 September 2023 / Accepted: 25 September 2023 / Published online: 18 October 2023

Abstract Geodynamic mechanism responsible for the generation of Silurian granitoids and the tectonic evolution of the Qilian orogenic belt remains controversial. In this study, we report the results of zircon U–Pb age, and systematic whole-rock geochemical data for the Haoquangou and Liujiaxia granitoids within the North Qilian orogenic belt and the Qilian Block, respectively, to constrain their petrogenesis, and the Silurian tectonic evolution of the Qilian orogenic belt. Zircon U–Pb ages indicate that the Haoquangou and Liujiaxia intrusions were emplaced at 423 ± 3 Ma and 432 ± 4 Ma, respectively. The Haoquangou granodiorites are calc-alkaline, while the Liujiaxia granites belong to the high-K calc-alkaline series. Both are peraluminous in composition and have relatively depleted Nd isotopic [$\varepsilon_{Nd}(t)$ = (− 3.9 – + 0.6)] characteristics compared with regional basement rocks, implying their derivation from a juvenile lower crust. They show adakitic geochemical characteristics and were generated by partial melting of thickened lower continental crust. Post-collisional extensional regime related to lithospheric delamination was the most likely geodynamic mechanism for the generation of the Haoquangou granodiorite, while the Liujiaxia granites were generated in a compressive setting during continental collision between the Qaidam and Qilian blocks.

Keywords Silurian adakitic granitoids · Petrogenesis · Tectonic setting · Qilian Orogenic Belt

✉ Jiao-Long Zhao
jlz@lzu.edu.cn

✉ Pei-Qing Hu
hupq@lzu.edu.cn

Xiao-Jun Huang
hxj606247@126.com

Zhen-Xi Yang
yangyyr@163.com

Ying Fan
fanying0525@163.com

Er-Teng Wang
wanget19@lzu.edu.cn

Fu-Bo Yang
yangfb20@lzu.edu.cn

Jing-Yu Zhang
zhangjingyu2020@lzu.edu.cn

[1] School of Earth Sciences, Key Laboratory of Mineral Resources in Western China (Gansu Province), Lanzhou University, Lanzhou 730000, China

[2] Nuclear Industry 247 Brigade, Tianjin North China Geological Survey Bureau, Tianjin 301800, China

[3] Fourth Institute of Geological and Mineral Exploration of Gansu Provincial Bureau of Geology and Mineral Resources, Jiuquan 735000, China

1 Introduction

Voluminous intermediate-acid igneous rocks are in the orogenic belts worldwide, especially during post-collisional periods (Liégeois 1998). These rocks usually range from tholeiitic, calc-alkaline, to high-K calc-alkaline in compositions, even with the occurrence of alkaline-peralkaline magmatism in the final stages of orogeny, and are commonly dominated by high-K calc-alkaline rocks (Liégeois 1998; Benito et al. 1999; Eyal et al. 2010; Litvinovsky et al. 2011). It has been recognized that their geochemical compositions invariably point to characteristics of source regions, conditions of partial melting, and

magma processes (Ma et al. 2016; Moyen 2009; Sisson et al. 2005). However, some geotectonic settings will be more propitious to generate certain types of magmatism (Eyal et al. 2010; Bonin 2007; Dall'Agnol et al. 2012). The corresponding rock associations thus usually show special temporal and spatial zoning, and play an important role in the reconstruction of the evolutionary histories of orogenic belts (Barbarin 1999; Eyuboglu et al. 2011; Zhao et al. 2016). On the other hand, generation of the intermediate-acid igneous rocks in the convergent plate margins is generally related to the partial melting of subducting slabs, the overlying mantle wedge, as well as arc crust, and have been considered to play a significant role in the growth of continental crust (Huang et al. 2015; Mo et al. 2008; Nagel et al. 2012; Niu et al. 2013). These magmatic rocks in the orogenic belt thus record indispensable information on crust-mantle recycling and can provide insight into the continental crustal growth and reworking.

The Qilian orogenic belt located on the northern margin of the Tibet Plateau in NW China records the complex histories from oceanic subduction to the ultimate continental collision during the Paleozoic (Fig. 1). It composes of the North Qilian orogenic belt, the Qilian Block, and the North Qaidam-ultrahigh pressure metamorphic (NQ-UHPM) belt from northeast to southwest (Fig. 1). Early Paleozoic magmatism was intense and widespread in the Qilian orogeny, and usually viewed as the products of subduction of oceanic crust and subsequent continental collision (Song et al. 2013, 2014; Wang et al. 2019; Zhao et al. 2021, 2022). However, the geodynamic mechanism responsible for the generation of Silurian granitoids and the corresponding tectonic evolution of the Qilian orogenic belt remain highly controversial (Song et al. 2013, 2014; Zhao et al. 2021; Tung et al. 2016).

In this study, we present new geochronological and geochemical data for the high-K calc-alkaline Liujiaxia granite and calc-alkaline Haoquangou granodiorite from the eastern Qilian Block and North Qilian orogenic belt, respectively (Fig. 1a). This study aims to place constraints on their petrogenesis, and the tectonic evolution of the Qilian orogenic belt.

2 Geological setting

The Qilian orogenic belt is generally regarded as the northernmost orogenic collage of the Proto-Tethys domain (Song et al. 2013; Li et al. 2018; Yao et al. 2021; Yu et al. 2021). It lies between the Alxa Block and the Qaidam Block–West Qinling orogenic belt and is offset by the Altyn-Tagh Fault to the northwest (Fig. 1a). The North Qilian orogenic belt could be divided into three subparallel tectonic-magmatic subunits, i.e., the northern back-arc ophiolite belt (ca. 490–449 Ma), the middle arc magmatic belt (ca. 520–440 Ma), and the southern ophiolite belt (ca. 550–496 Ma, Song et al. 2013; Xia et al. 2016; Chen et al. 2023; Zhang et al. 2019, Fig. 1). Precambrian basement is composed of the Lower Paleoproterozoic Beidahe, Middle-Upper Proterozoic Jingtieshan and Neoproterozoic Daliugou and Baiyanggou Formations, and all of them are unconformably overlain by younger strata. The Paleozoic granitoids are widely distributed in the North Qilian Orogenic belt, and are dominated by S- and I-type, and subordinate A-type granitoid. Some of the S- and I-type granitoids show adakitic geochemical affinities, and could be further divided into high- and low-Mg subtypes (Wang et al. 2019; Xia et al. 2016; Chen et al. 2023; Zhang et al. 2019). The Qilian Block is mainly composed of basement rocks, Early Paleozoic granitoids, and Phanerozoic sediment covers. The basement of the Qilian Block is dominated by Proterozoic low-grade metamorphic rocks, including the Xinlongshan, Maxianshan, Huangyuan, Hualong, and Yemananshan Groups. Early Paleozoic magmatic rocks within the Qilian Block are composed of high-K calc-alkaline S-type and I-type granitoids, with minor A-type granitoids and mafic rocks (Cui et al. 2019; Tung et al. 2016; Zhao et al. 2022). The basement rocks and granitoids in the Qilian Block are unconformably overlain by the Phanerozoic sediment covers. In the eastern Qilian Block, the widespread granitoids are temporally and spatially associated with gabbro, forming characteristic gabbro-granitoid associations, such as the Bamishan (ca. 438–459 Ma) and Heishishan (ca. 438–447 Ma) complexes (Yang et al. 2021). These granitoids generally show adakitic geochemical characteristics, such as the Shichuan and Hejiashan plutons (Tung et al. 2016; Zhao et al. 2022). Especially, granitoid intrusions in the eastern Qilian Block appear to constitute a Nord-East direction chain (Fig. 1a). The NQ-UHPM belt was formed during a collisional orogenic event, and is characterized by ultrahigh-pressure metamorphic rocks (Xia et al. 2016; Yang et al. 2020).

3 Petrography

The Liujiaxia granite pluton is about 8 km^2 in size and located in the eastern section of the Qilian Block (Fig. 1b). It intrudes into the Precambrian metamorphic rocks of the Maxianshan Group and is partly unconformably overlain by the sedimentary rocks of the Mesozoic Hekou Group. It consists predominantly of fresh, medium- to coarse-grained granodiorites. The U–Pb zircon age, for the granites is 432 ± 4 Ma (Yang et al. 2021). The major minerals are ~50–55 vol% plagioclase (1–4 mm), ~20–30 vol% quartz (0.5–1.5 mm), ~10–15 vol% K-feldspar (1 to 3 mm), and ~5–10 vol% biotite (0.1–0.5 mm) (Fig. 2a, c).

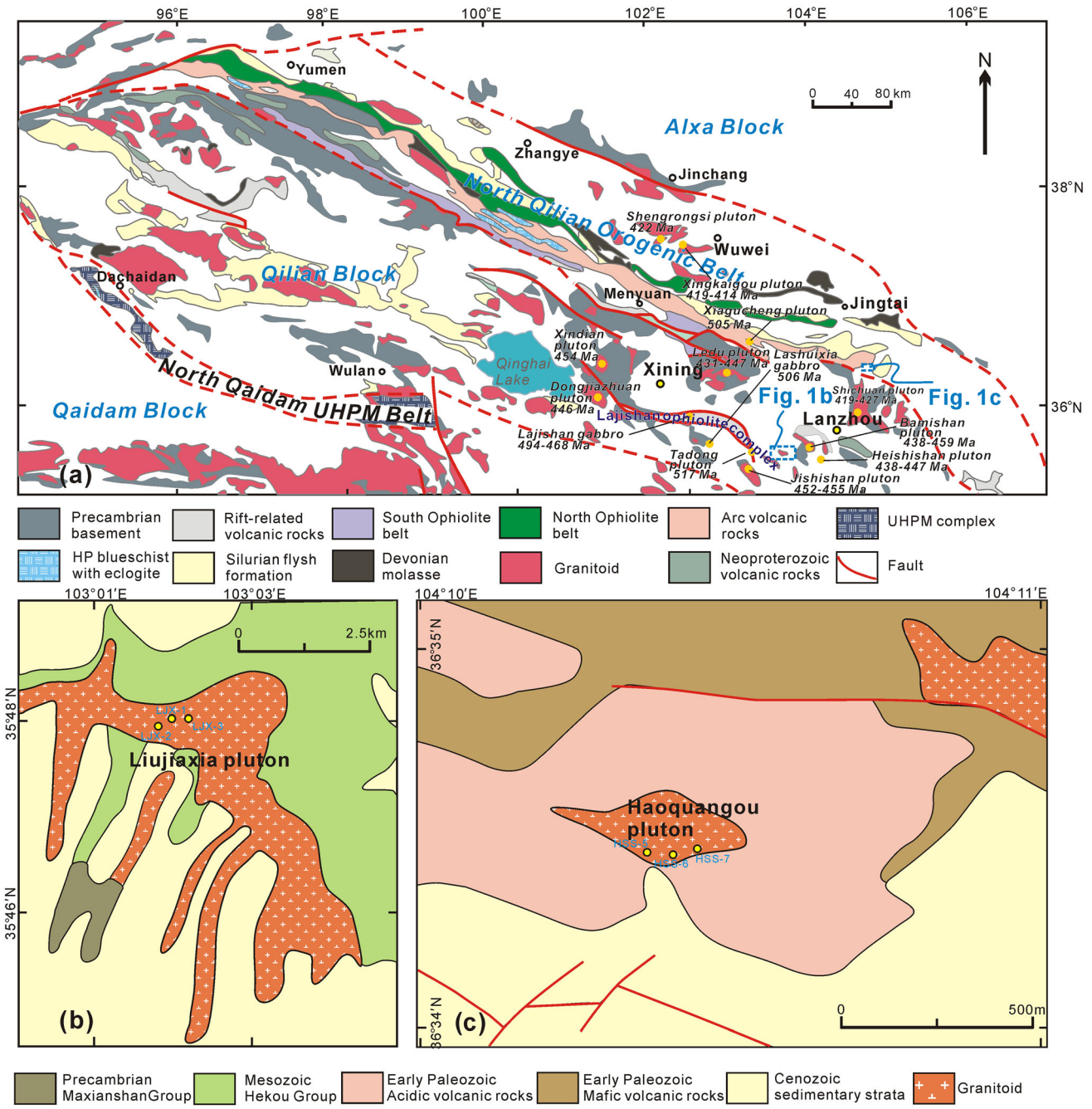

Fig. 1 **a** Simplified geological map of the Qilian orogenic belt showing the localities of the Haoquangou and Liujiaxia plutons (modified after Xia et al. 2016 and Zhao et al. 2022). **b** Geological map of the Liujiaxia granitic pluton (modified after Yang et al. 2021). **c** Geological map of the Haoquangou pluton (modified after Zhao et al. 2013)

Accessory minerals include apatite, zircon, allanite, and Fe–Ti oxides (Fig. 2d). Plagioclase usually occurs as subhedral–euhedral laths with well-developed twinning and compositional zoning. Biotite varies in form from anhedral grains to subhedral blade-shaped crystals (Fig. 2c). K-feldspar is mostly subhedral with tartan twinning (Fig. 2c).

The Haoquangou granodiorite pluton crops out in north Baiyin City, Gansu Province (Fig. 1c) and is closely related to regional Cu-Au mineralization. The pluton has

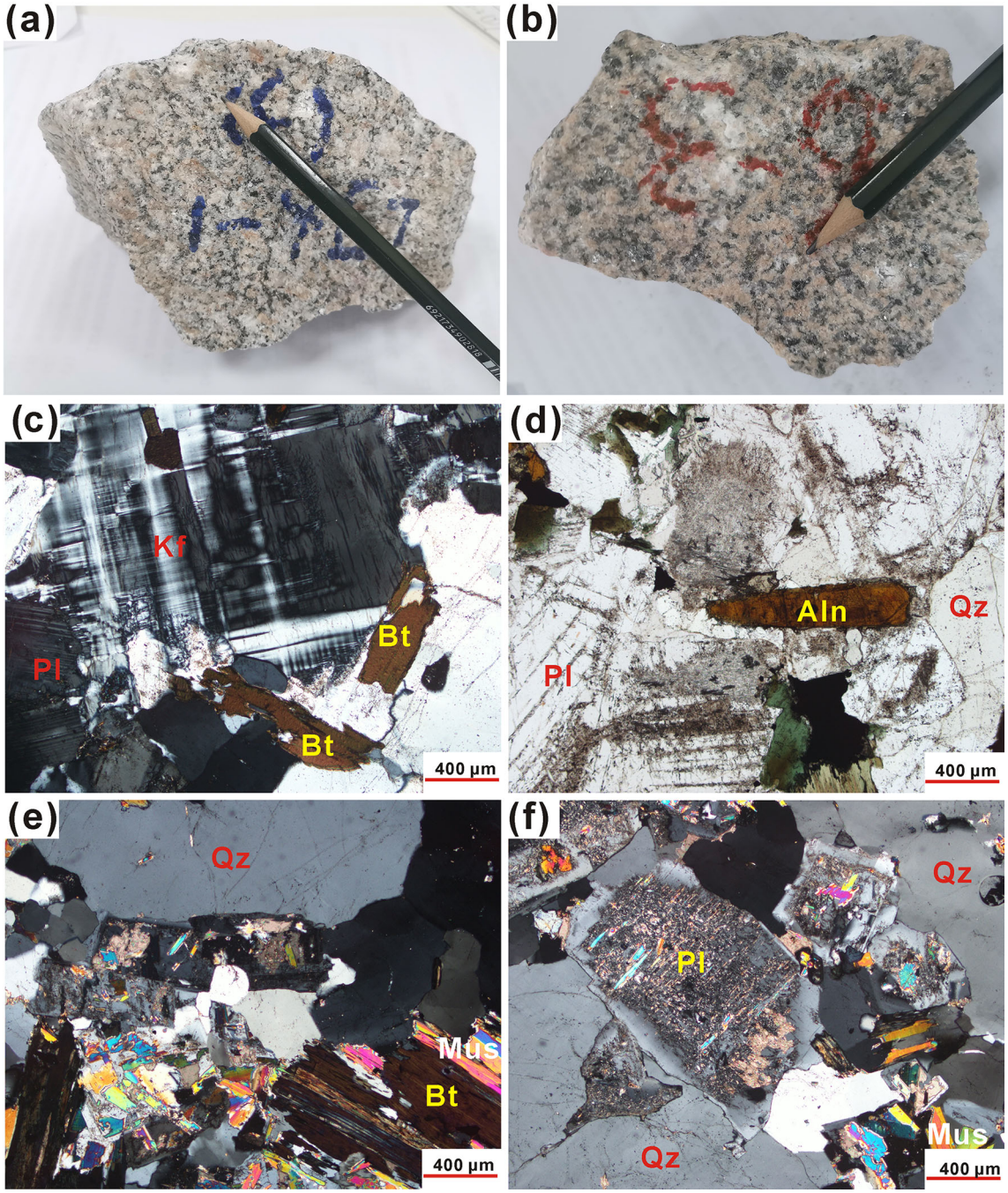

Fig. 2 Macroscopic photos and thin section images of rocks from the Liujiaxia and Haoquangou plutons. **a** Field photograph of Liujiaxia granite specimen. **b** Field photograph of Haoquangou granodiorite specimen. **c**, **d** Cross- and plane-polarized, transmitted-light images of granites from the Liujiaxia pluton. **e**, **f** Cross-polarised, transmitted-light images of granitoids from the Haoquangou pluton. Mineral abbreviation: Qz, quartz; Kf, K-feldspar; Pl, plagioclase; Bt, biotite; Mus, muscovite; Aln, allanite

intruded into the Cambrian–Ordovician arc volcanic rocks, with an outcrop area of ca. 0.03 km^2. It consists predominantly of medium-grained granodiorites that are fresh, and have equigranular texture (Fig. 2b). They are mainly composed of ~20–25 vol% quartz (0.5 to 4 mm), ~50–55 vol% plagioclase (1–2 mm), ~10–15 vol% K-feldspar (1–2 mm), ~10–15 vol% biotite (0.5–1 mm) and ~5 vol% muscovite (0.1–0.5 mm), with accessory minerals of zircon, apatite and Fe–Ti oxides (Fig. 2e, f).

Table 1 Zircon LA–ICP–MS U–Pb isotopic data of the Haoquangou granodiorite

Spot no.	Th/U	Isotopic ratios						Ages (Ma)			
		$^{207}Pb/^{206}Pb$		$^{207}Pb/^{235}U$		$^{206}Pb/^{238}U$		$^{207}Pb/^{235}U$		$^{206}Pb/^{238}U$	
		Ratio	± 1σ	Ratio	± 1σ	Ratio	± 1σ	Age	± 1σ	Age	± 1σ
Haoquangou granodiorite											
HSS-6, coordinate: N36°34′48″ E104°10′22″											
HSS6-01	1.02	0.06147	0.00139	0.57566	0.01265	0.06795	0.00086	462	8	424	5
HSS6-02	0.75	0.05549	0.00100	0.51515	0.00928	0.06735	0.00082	422	6	420	5
HSS6-03	0.74	0.05539	0.00098	0.51394	0.00913	0.06730	0.00083	421	6	420	5
HSS6-04	0.83	0.05983	0.00133	0.55541	0.01204	0.06735	0.00086	449	8	420	5
HSS6-05	0.78	0.05616	0.00097	0.52303	0.00899	0.06756	0.00080	427	6	421	5
HSS6-06	0.74	0.05464	0.00091	0.50937	0.00850	0.06764	0.00079	418	6	422	5
HSS6-07	0.69	0.05731	0.00152	0.53800	0.01380	0.06812	0.00091	437	9	425	5
HSS6-08	0.68	0.05675	0.00126	0.53303	0.01166	0.06814	0.00088	434	8	425	5
HSS6-09	1.19	0.06641	0.00103	0.61938	0.01007	0.06765	0.00084	489	6	422	5
HSS6-10	0.67	0.05734	0.00206	0.54187	0.01868	0.06853	0.00108	440	12	427	7
HSS6-11	0.78	0.05953	0.00116	0.55437	0.01067	0.06755	0.00083	448	7	421	5
HSS6-12	0.81	0.05995	0.00136	0.57389	0.01270	0.06943	0.00089	461	8	433	5
HSS6-13	0.69	0.05722	0.00096	0.53472	0.00921	0.06778	0.00083	435	6	423	5
HSS6-14	0.84	0.05705	0.00114	0.52726	0.01054	0.06704	0.00084	430	7	418	5
HSS6-15	0.71	0.05723	0.00108	0.53306	0.01016	0.06757	0.00084	434	7	421	5

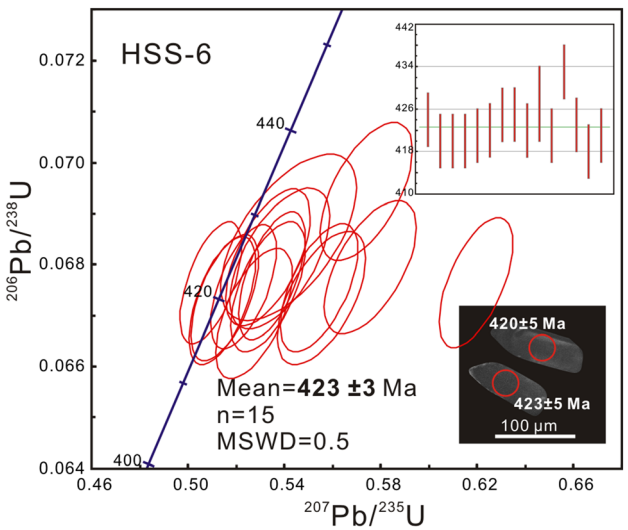

Fig. 3 CL images of representative zircon grains and U–Pb concordia diagram for the Haoquangou granodiorite

4 Analytical methods

4.1 Zircon U–Pb dating

Sample HSS-6 for the Haoquangou granodiorite in this study is selected for zircon U–Pb dating. Cathodoluminescence images (CL) of zircons in the pluton were obtained using a Gatan Mini CL detector attached to a JSM-6510 scanning electron microscope at the Key Laboratory of Mineral Resources, Lanzhou University, Lanzhou, China.

Zircon U–Pb isotopic compositions were determined by laser ablation–inductively coupled plasma–mass spectrometry (LA–ICP–MS) at the State Key Laboratory for Mineral Deposits Research (SKLMDR), Nanjing University, China. Analyses were carried out using a beam diameter of 32 μm and a repetition rate of 5 Hz. The instruments and analytical processes used are similar to those outlined in Zhao et al. (2021). A homogeneous GJ-1 standard zircon was used as a primary standard for calibration of the mass discrimination of the mass spectrometer and residual elemental fractionation. A Zircon Mud Tank was used as a secondary standard to monitor instrument performance. In this study, the standards Mud Tank and GJ-1 yielded weighted mean $^{206}Pb/^{238}U$ ages of 728 ± 4 Ma (n = 5) and 600 ± 3 Ma (n = 15), respectively, all of which are consistent with the recommended $^{206}Pb/^{238}U$ ages of 732 ± 5 Ma (Black and Gulson. 1978) and 599.8 ± 4.5 Ma (Yuan et al. 2008). Systematic sources of uncertainty are 1.9% for $^{206}Pb/^{238}U$ and 1.3% for $^{207}Pb/^{206}Pb$. Common Pb correction was done following the method of Andersen (2002). Isoplot 4.15 software was

Table 2 Bulk rock major (wt%) and trace element (ppm) analyses of representative samples from the Liujiaxia and Haoquangou plutons

Rock type	Liujiaxia granite								Haoquangou granodiorite					
Sample	LJX-1	LJX-2	LJX-3	Q1219*	Q1220*	Q1221*	Q1223*	Q1224*	HSS-5	HSS-6	HSS-7	Q1210#	Q1211#	Q1213#
SiO_2	69.71	71.95	69.72	69.58	69.58	71.53	70.94	70.86	68.22	69.89	69.10	69.37	69.19	70.10
TiO_2	0.35	0.31	0.38	0.34	0.32	0.42	0.28	0.29	0.25	0.27	0.29	0.26	0.28	0.27
Al_2O_3	15.21	15.18	15.41	15.18	15.32	13.56	14.73	14.97	14.44	14.67	14.82	14.99	15.27	14.55
$Fe_2O_3^T$	2.22	2.01	2.46	2.29	2.24	2.82	1.96	1.92	2.11	2.42	2.53	2.18	2.28	2.29
MnO	0.04	0.03	0.05	0.05	0.04	0.06	0.04	0.05	0.04	0.04	0.04	0.03	0.04	0.03
MgO	0.76	0.66	0.79	0.73	0.76	1.03	0.60	0.60	0.89	1.06	1.09	0.99	1.03	1.04
CaO	2.49	2.00	2.50	2.30	2.33	1.85	2.09	2.16	3.06	2.78	2.85	2.54	2.64	2.41
Na_2O	4.44	4.16	4.46	4.11	4.27	3.41	4.19	4.38	3.26	3.98	3.99	4.01	4.18	3.85
K_2O	2.89	3.77	3.12	3.36	3.19	3.16	3.19	3.19	2.61	1.98	2.01	2.16	2.13	2.05
P_2O_5	0.13	0.13	0.16	0.13	0.13	0.15	0.10	0.10	0.13	0.09	0.11	0.09	0.09	0.09
LOI	0.95	0.76	0.38	0.57	0.72	1.06	0.69	0.57	4.00	1.89	2.78	2.53	0.74	2.72
Total	99.20	100.96	99.42						99.01	99.06	99.62			
K_2O/Na_2O	0.65	0.91	0.70	0.82	0.75	0.93	0.76	0.73	0.80	0.50	0.50	0.54	0.51	0.53
A/CNK	1.02	1.04	1.01	1.04	1.04	1.09	1.04	1.03	1.05	1.07	1.06	1.10	1.09	1.12
Mg#	40.41	39.41	38.88	38.71	40.19	41.98	37.75	38.23	45.52	46.46	46.05	47.36	47.23	47.36
Sc	2.74	2.82	3.73	4.12	3.75	5.20	3.80	3.70	4.46	5.17	3.77			
V	31.6	30.9	33.5	26.9	26.7	31.1	22.7	22.20	44.1	42.8	45.8			
Cr	8.69	12.34	8.58	2.94	3.03	3.85	2.74	2.96	7.65	5.63	5.89	3.33	3.30	3.58
Co	4.08	3.43	4.17	98.4	82.5	79.4	97.9	99.7	5.94	6.48	6.15	80.4	83.4	88.2
Ni	2.48	5.47	4.73	2.83	2.94	2.76	3.07	3.13	7.26	5.89	7.01	3.96	3.45	3.91
Ga	17.3	17.8	18.2	19.5	19.1	18.3	18.8	18.8	15.5	15.5	15.1			
Cs	1.50	3.75	2.39	2.23	5.08	4.94	4.61	1.79	1.76	2.23	2.44	2.23	3.43	2.83
Rb	56.2	77.8	67.6	92.2	90.6	98.9	98.9	84.9	71.2	55.7	37.0	68.9	65.2	69.9
Ba	1583	2015	1402	1554	1492	997	1098	1227	694	1012	826	652	633	640
Th	13.5	15.8	13.1	13.7	13.4	10.8	11.8	9.64	7.63	9.63	8.09	7.53	8.28	8.39
U	1.08	0.89	0.84	1.16	1.15	1.01	1.76	5.35	2.04	3.98	1.94	2.18	8.46	2.65
Ta	0.52	0.70	0.32	0.98	0.94	0.66	1.33	1.08	0.54	0.41	0.37	0.62	0.59	1.43
Nb	7.62	8.97	8.78	12.4	10.8	15.3	12.0	11.4	8.55	6.06	5.35	5.39	5.90	7.47
Pb	26.3	30.8	30.4	34.6	32.2	33.7	35.5	35.5	20.1	27.4	16.0	12.9	16.9	12.3
Sr	650	578	608	657	655	478	550	597	370	508	376	369	435	376
Zr	162	146	163	180	178	177	155	139	76.3	76.3	83.5	91.9	99.3	93.4
Hf	4.49	4.33	4.63	4.30	4.33	4.27	3.92	3.40	2.44	2.42	2.60	2.38	2.53	2.34
Y	7.30	7.18	5.30	10.1	9.93	7.20	10.40	9.60	4.01	4.20	4.41	4.29	4.67	4.44
La	56.7	44.7	53.2	53.3	54.2	22.1	35.5	38.9	16.5	18.5	15.8	14.7	15.9	15.8
Ce	95.7	83.7	89.5	94.5	84.4	34.8	68.4	69.5	28.6	32.8	27. 6	25.6	27.9	27.4
Pr	10.39	8.53	10.03	9.41	9.59	4.17	6.51	6.92	2.96	3.39	2.96	2.58	2.82	2.76
Nd	34.7	28.0	34.2	31.1	30.1	13.4	20.7	22.5	10.2	11.6	10.3	8.63	9.36	9.22
Sm	4.49	3.70	4.50	4.58	4.11	2.25	3.37	3.12	1.56	1.78	1.62	1.58	1.63	1.54
Eu	1.62	1.72	1.52	1.05	1.02	0.74	0.84	0.81	0.72	0.89	0.76	0.46	0.44	0.43
Gd	4.81	4.11	4.51	2.55	2.21	1.67	2.09	2.08	1.75	2.04	1.82	1.14	1.17	1.04
Tb	0.44	0.40	0.39	0.34	0.33	0.24	0.29	0.29	0.19	0.20	0.20	0.16	0.16	0.15
Dy	1.62	1.60	1.27	1.74	1.68	1.23	1.74	1.55	0.82	0.87	0.91	0.76	0.86	0.72
Ho	0.27	0.27	0.20	0.31	0.32	0.21	0.31	0.28	0.15	0.15	0.16	0.15	0.15	0.14
Er	0.89	0.88	0.66	0.79	0.82	0.58	0.86	0.79	0.46	0.45	0.48	0.36	0.40	0.33
Tm	0.10	0.11	0.07	0.12	0.12	0.08	0.13	0.11	0.06	0.06	0.06	0.06	0.06	0.06

Table 2 continued

Rock type	Liujiaxia granite								Haoquangou granodiorite					
Sample	LJX-1	LJX-2	LJX-3	Q1219*	Q1220*	Q1221*	Q1223*	Q1224*	HSS-5	HSS-6	HSS-7	Q1210#	Q1211#	Q1213#
Yb	0.66	0.73	0.46	0.71	0.85	0.51	0.87	0.78	0.40	0.37	0.41	0.37	0.41	0.32
Lu	0.10	0.11	0.08	0.11	0.13	0.08	0.15	0.12	0.06	0.06	0.06	0.05	0.06	0.04
La/Yb	85.98	61.64	115.80	75.07	63.76	43.33	40.80	49.87	39.73	38.78	49.38	41.10	50.10	38.70
Sr/Y	89.11	80.51	114.69	65.05	65.96	66.39	52.88	62.19	86.01	93.15	84.68	92.28	121.08	85.34

LOI, loss on ignition; A/CNK = $Al_2O_3/(CaO + Na_2O + K_2O)$ molar; Mg# =100 × Mg/(Mg + Fe); $Fe_2O_3^T$, total Fe expressed as Fe_2O_3; t_{Zr} (°C). *Data from Yang et al. (2021), #Data from Yang et al. (2020a)

used for weighted-mean calculations and for plotting concordia diagrams.

4.2 Whole-rock major and trace element, and Sr–Nd isotope analyses

Fresh rock samples were crushed to powders of 200 mesh in an agate ring mill. Whole-rock major elements were analyzed using a Thermo Scientific ARL 9900 X-ray fluorescence (XRF) spectrometer at SKLMDR, China, following a method similar to Zhao et al. (2021). RMG-2, BCR-2, and BHVO-2 standards were used for quality control. The analytical precision was estimated to be less than 10% for all major oxides and less than 1% for the majority of oxides. Whole-rock trace element contents were measured using a Finnigan Element II ICP–MS at SKLMDR, China. Detailed analytical procedures followed by Gao et al. (2003), yield analytical precisions that are better than 10% for all trace elements, with the majority being better than 5%.

Whole-rock Sr–Nd isotopic compositions were determined at the Tianjin Shangnuo Geological Technology Co. Ltd., Tianjin, China. The analytical conditions and procedures used during this study are similar to those described in Zhao et al. (2021). Raw data of isotopic ratios were corrected for mass fractionation by normalizing to $^{86}Sr/^{88}Sr = 0.1194$ for Sr and $^{146}Nd/^{144}Nd = 0.7219$ for Nd. International isotopic standards (NIST SRM 987 for Sr and JNdi-1 for Nd) were periodically analyzed to correct instrumental drift. Geochemical reference material AGV-2 was used for quality control purposes. During the analysis period, the standard solution of AGV-2 yielded an average $^{87}Sr/^{86}Sr$ value of 0.703984 ± 0.000006 (n = 3) and an average $^{143}Nd/^{144}Nd$ ratio of 0.512795 ± 0.000005 (n = 3).

5 Results

5.1 Zircon U–Pb ages

Zircon CL images and LA–ICP–MS zircon U–Pb dating results for sample HSS-6 from the Haoquangou pluton are listed in Table 1 and shown in Fig. 3. The zircon grains extracted from the Haoquangou granodiorite are transparent and colorless to pale yellow, and have lengths of 60–120 μm and length/width ratios of 1:1 to 3:1. They show weak or clear magmatic oscillatory zoning in the CL images (Fig. 3) and mostly have relatively high Th/U ratios of 0.67–1.19. Fifteen analyses from sample HSS-6 yield concordant $^{206}Pb/^{238}U$ ages ranging from 418 to 433 Ma. The weighted mean of 423 ± 3 Ma (MSWD = 0.5) (Fig. 3) is interpreted as the crystallization age of the Haoquangou granodiorite.

5.2 Whole-rock major and trace element geochemistry

Whole-rock major and trace-element compositions are given in Table 2. All of the studied samples from the Haoquangou and Liujiaxia plutons show limited chemical variation, have high SiO_2 contents varying from 68.22 to 70.10 wt% and 69.58 to 71.95 wt%, respectively, and all fall into the subalkaline series field in a total alkali versus silica (TAS) diagram (Fig. 4a). The Liujiaxia granites have high alkali contents, are enriched in K_2O with K_2O/Na_2O weight ratios of 0.65–0.93 and can be classified as high-K calc-alkaline rocks (Fig. 4b). They are weakly peraluminous in composition with A/CNK ratios of 1.01 to 1.09 (Fig. 4c). In contrast, the Haoquangou granodiorites have relatively low alkali contents, are high in Na_2O, with K_2O/Na_2O weight ratios of 0.50–0.80, and can be classified as calc-alkaline series (Fig. 4b). They are weakly to strongly peraluminous with relatively high A/CNK values of 1.05–1.12 (Fig. 4c).

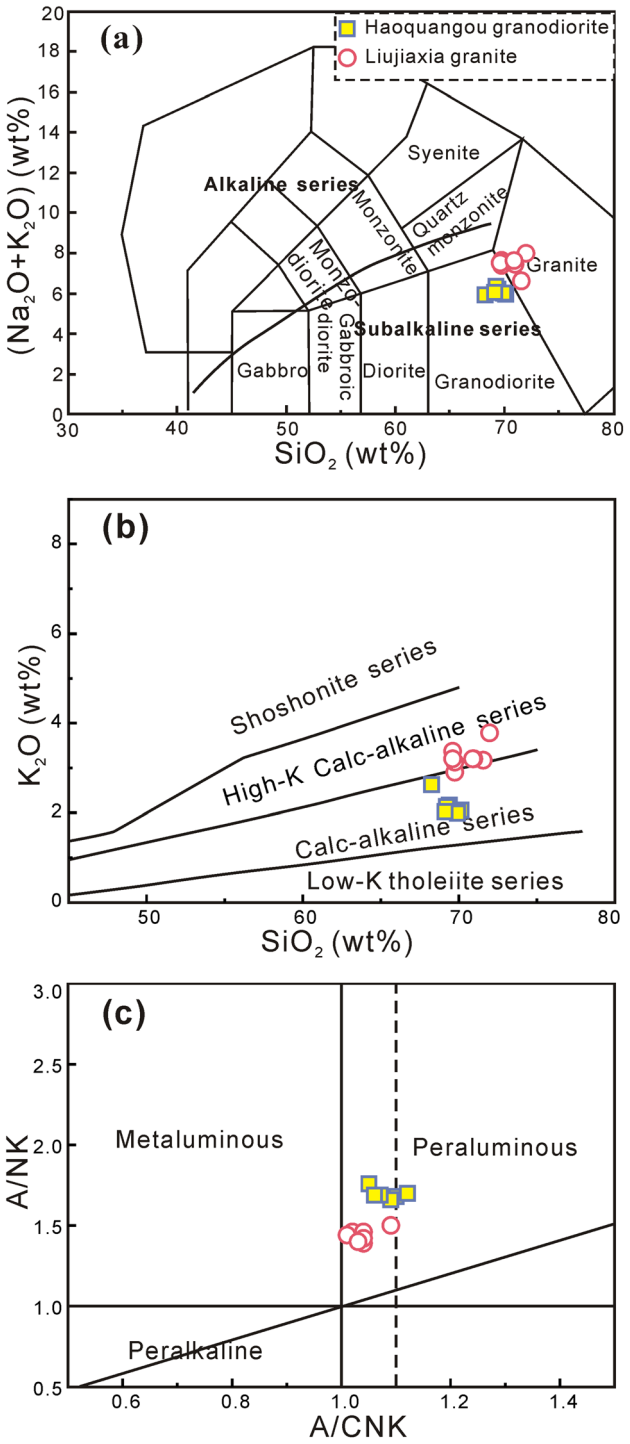

Fig. 4 Geochemical classification of representative samples from the Liujiaxia and Haoquangou plutons. **a** Total alkali versus silica diagram (after Middlemost 1994); with the thick solid line from (after Irvine and Baragar 1971). **b** K_2O versus SiO_2 diagram (after Peccerillo and Taylor 1976). **c** A/NK vs. A/CNK diagram (after Maniar and Piccoli 1989; Chappell and White 1974)

Granitoids from both the Liujiaxia and Haoquangou plutons show similarly fractionated chondrite-normalized rare earth element (REE) patterns and are marked by significant light REE (LREE) enrichment, strongly heavy REE depletion, and insignificant to positive Eu anomalies, with La/Yb ratios of 40.8–115.8 and 38.7–50.1, and Eu/Eu* values of 0.94–1.35 and 0.97–1.43, respectively (Fig. 5). On primitive mantle normalized multi-element diagrams, they are enriched in large ion lithophile elements (LILEs; e.g., Cs, K, Th), and depleted in Ta, Nb, P, and Ti, with slightly positive Zr-Hf anomalies (Fig. 5). Of note, the Liujiaxia granites have higher total REE, Ba, Zr, and Hf concentrations than those of the Haoquangou granodiorites (Fig. 5).

5.3 Whole-rock Rb–Sr and Sm–Nd isotopes

Representative whole-rock Sr–Nd isotopic analyses for the Liujiaxia and Haoquangou plutons are given in Table 3 and illustrated in Fig. 7. The Liujiaxia granites have relatively homogeneous initial $^{87}Sr/^{86}Sr$ ratios [$(^{87}Sr/^{86}Sr)_i$] of 0.7071–0.7075, and $\varepsilon_{Nd}(t)$ values of − 3.9 to − 1.4, with two-stage Nd model ages ranging from 1.49 to 1.29 Ga. In contrast, the Haoquangou granodiorites have lower ($^{87}Sr/^{86}Sr)_i$ ratios (0.7053–0.7059) and higher $\varepsilon_{Nd}(t)$ values (− 1.4 to + 0.6) than the Liujiaxia granites (Fig. 7). The corresponding two-stage Nd model ages are strikingly younger, ranging from 1.28 to 1.12 Ga.

6 Discussion

6.1 Petrogenesis of the Liujiaxia and Haoquangou adakitic rocks

The term “adakite” refers to a group of intermediate–felsic volcanic and plutonic rocks, which are geochemically characterized by depletions in Y and heavy REEs, high Sr/Y and La/ Yb ratios (Castillo et al. 1999; Defant and Drummond 1990). Alternative genetic models have been suggested to explain the origins of adakitic rocks, including (1) fractional crystallization of parental basaltic magmas (Castillo et al. 1999; Dai et al. 2017); (2) their adakitic signature is inherited from source rocks (Xie et al. 2023); (3) mixing between crust- and mantle-derived magmas (Chen et al. 2013); (4) partial melting of thickened/delaminated lower crust (Atherton and Petford 1993; Chung et al. 2003); or (5) partial melting of subducted oceanic slabs (Defant and Drummond 1990). The Liujiaxia and Haoquangou granitoids are characterized by strong depletion in heavy REEs and Y, and high Sr/Y, La/Yb, and Sm/Yb ratios, and show insignificant to moderate positive Eu anomalies with Eu/Eu* of 0.94–1.43. All samples plot in

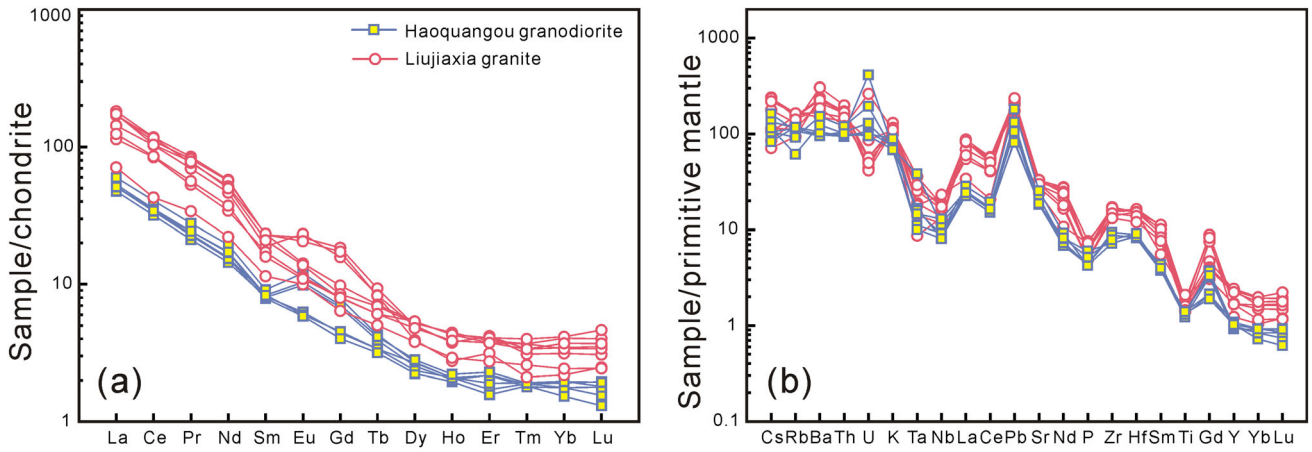

Fig. 5 Chondrite-normalized REE patterns (**a**) and primitive-mantle-normalized trace element variation diagrams (**b**) of rocks from the Liujiaxia and Haoquangou plutons. The data for chondrite and primitive mantle are from Boynton (1984) and McDonough and Sun (1995), respectively

the field of the adakite in the Sr/Y vs. Y and $(La/Yb)_N$ vs. $(Yb)_N$ plots (Fig. 6a, b). These suggest that the Liujiaxia and the Haoquangou granitoids in the Qilian orogenic belt belong to adakitic rocks.

Granitoids from the Liujiaxia and Haoquangou plutons have relatively homogeneous whole-rock element composition, initial $^{87}Sr/^{86}Sr$ and $\varepsilon_{Nd}(t)$ values, and do not display a mixing trend. Moreover, they show significantly lower MgO, Ni, and Cr contents, and Mg# values (37.8–47.4) than those of the adakitic rocks formed by magma mixing of crust- and mantle-derived magma (Mg# values > 52, MgO > 3 wt%, Chen et al. 2013). These, combined with the common absence of mafic, microgranular enclaves, and petrographic disequilibrium textures within the two plutons, imply that magma mixing did not play a major role during their generation. Spatially, the studied granitoids are not associated with contemporaneous massive mafic magmas and display uniform REE patterns. Moreover, they display almost constant or decreasing La/Yb ratios with increasing SiO_2 contents (Fig. 6c), suggesting insignificant fractionations of amphibole and garnet during their generation because both amphibole and garnet preferentially incorporate HREE compared to LREE. Their Dy/Yb ratios are almost constant with increasing SiO_2 contents (Fig. 6d). Therefore, the Liujiaxia and Haoquangou granitoids could not be derived from primary basaltic magma by fractional crystallization.

Previous studies have identified that some of the Early Paleozoic granitoid within the Qilian orogenic belt show non-adakitic geochemical characteristics (Tung et al. 2016; Zhang et al. 2019; Zhao et al. 2022), thereby precluding the possibility of the adakitic geochemical compositions of the Liujiaxia and Haoquangou plutons inherited from their source rocks. Moreover, the adakitic magmas derived by partial melting of basaltic ocean crust are commonly sodic, with K_2O/Na_2O ratios of ~0.4 (Defant and Drummond 1990; Martin 1999). The K_2O/Na_2O ratios of the Liujiaxia and Haoquangou granitoids (0.50–0.93) are higher than those of the slab-derived adakites but similar to those of the thickened lower continental crust or delaminated lower continental crust-derived adakitic rocks. Their CaO/Al_2O_3 ratios (0.13–0.21) are significantly lower than those derived from partial melting of subducted oceanic crust (> 0.2, Li et al. 2016, and references therein). Their Sr–Nd isotopic compositions are more evolved than those of the Early Paleozoic ophiolites (Fig. 7). In addition, they show significantly lower Cr and Ni concentrations compared with those of the slab-derived melts (Fig. 6e, f). Therefore, the granitoids from the Liujiaxia and Haoquangou plutons were likely generated by partial melting of the thickened lower continental crust or delaminated lower continental crust, rather than a subducted oceanic crust.

The partial melting of delaminated lower continental crustal material in the mantle produces adakitic magmas with significantly elevated MgO (> 3 wt%), Cr, and Ni concentrations, and with high Mg# values because of interaction with the mantle (> 50; Hu et al. 2012; Rapp et al. 1999), different from those observed in the Liujiaxia and Haoquangou granitoids. Consequently, the geochemical data presented here indicate that the Liujiaxia and Haoquangou granitoids were derived directly from the partial melting of a thickened lower crust. Moreover, their peraluminous nature, relatively higher Na_2O contents, and more depleted Nd isotopic composition, further imply their derivation from juvenile lower crust. Their relatively large variation in Sr-Nd isotopic composition may have resulted from crustal contamination.

Both the Liujiaxia and Haoquangou granitoids are enriched in Ba, Sr, and Eu, depleted in HREEs and Y, and have high Sr/Y and La/Yb ratios with insignificantly or

Table 3 Whole-rock Rb–Sr and Sm–Nd isotopic data for the Haoquangou and Liujiaxia plutons

Sample No.	t(Ma)	Rb (ppm)	Sr (ppm)	$^{87}Rb/^{86}Sr$	$^{87}Sr/^{86}Sr$	$(^{87}Sr/^{86}Sr)_i$	Sm (ppm)	Nd (ppm)	$^{147}Sm/^{144}Nd$	$^{143}Nd/^{144}Nd$	$\varepsilon_{Nd}(t)$	T_{DM2}(Ga)
Haoquangou granodiorite												
HSS-6	223	55.7	508	0.31703	0.707761 ± 5	0.7059	1.78	11.62	0.0926	0.512379 ± 6	0.56	1.12
Q1210*	223	68.9	369	0.54020	0.708535 ± 4	0.7053	1.58	8.63	0.1106	0.512326 ± 11	− 1.44	1.28
Q1213*	223	69.9	376	0.53784	0.708676 ± 5	0.7054	1.54	9.22	0.1009	0.512399 ± 11	0.51	1.12
Liujiaxia granite												
LJX-1	432	56.2	650	0.25013	0.709054 ± 11	0.7075	4.49	34.68	0.0782	0.512230 ± 4	− 1.42	1.29
Q1219#	432	92.2	657	0.40606	0.710023 ± 6	0.7075	4.58	31.1	0.0890	0.512152 ± 5	− 3.54	1.46
Q1221#	432	98.9	478	0.59872	0.710762 ± 3	0.7071	2.25	13.4	0.1015	0.512171 ± 10	− 3.86	1.49
Q1224#	432	84.9	597	0.41149	0.710029 ± 5	0.7075	3.12	22.5	0.0838	0.512177 ± 8	− 2.76	1.40

*Data for the Haoquangou granodiorite are from Yang et al. (2020a); #Data for the Liujiaxia biotite granite are from Yang et al. (2021)

slightly positive Eu, suggesting the absence of residual plagioclase in the magma source. Partial melting experiments of mafic lower crust have indicated that melts with high Sr/Y and La/Yb ratios can be generated at pressures between 10.0 and 12.5 kbar without the need for a thickened crust (Qian and Hermann. 2013). Samples from the Liujiaxia and Haoquangou plutons plot along the trend of melts derived from the thickened crust (Fig. 8). They are strongly depleted in Y and the HREE with steep HREE patterns, and have high Y/Yb (9.89–14.23) and $(Ho/Yb)_N$ (1.04–1.27) ratios, suggestive of garnet-bearing residues during the partial melting as residual hornblende will generate melts with flat HREE patterns and Y/Yb ≈ 10 and $(Ho/Yb)_N \approx 1$ (Ge et al. 2002; Hu et al. 2012). Collectively, these further suggest that partial melting occurred in a thickened region of the lower continental crust (> 50 km).

6.2 Tectonic implications

The Qilian orogenic belt records a complete Neoproterozoic to Paleozoic tectonic history correlated with the Rodinia breakup and Gondwana assembly. The Paleozoic subduction, closure of ocean basin (s), and ultimate continental collision gave rise to voluminous ophiolites and intermediate-acidic intrusive rocks in the Qilian orogenic belt (Tung et al. 2016; Song et al. 2013; Xia et al. 2016). The existence of the Late Cambrian igneous rocks in the northern margin of the Qilian Block and the Lajishan ophiolite complex could not be well explained by the southward subduction of the North Qilian oceanic slab located between the Qilian Block and North Qilian orogenic belt (Zhao et al. 2021, 2022). The identification of ophiolite sequences and island arc volcanic rocks in the NQ-UHPM belt implies that there an ocean (namely, the South Qilian Ocean) between the Qilian Block and the Qaidam-West Qinling orogenic belt. Given the well-developed western Pacific-type trench–arc–basin system of the North Qilian orogenic belt (Song et al. 2013; Xia et al. 2016), these indicate that the formation of the Liujiaxia and Haoquangou plutons was related to the northward subduction of the South and North Qilian oceans, respectively.

The new zircon U–Pb age of 423 ± 3 Ma for the Haoquangou granodiorite is approximately coeval with the 414–422 Ma Shengrongsi and Xinkaigou A-type granites in the North Qilian orogenic belt, and ca. 433 Ma Jinchuan A-type granitites in adjacent Alxa Block, implying formation of the Haoquangou pluton in an extensional regime (Fig. 9) (Yang et al. 2018; Zhang et al. 2017). Existing studies have suggested that the voluminous Early Paleozoic adakitic rocks in the eastern part of the North Qilian orogenic belt, could be further divided into low-Mg and high-Mg subtypes (Tseng et al. 2009; Yu et al. 2015). Zircon U–Pb dating results indicate that the high-Mg

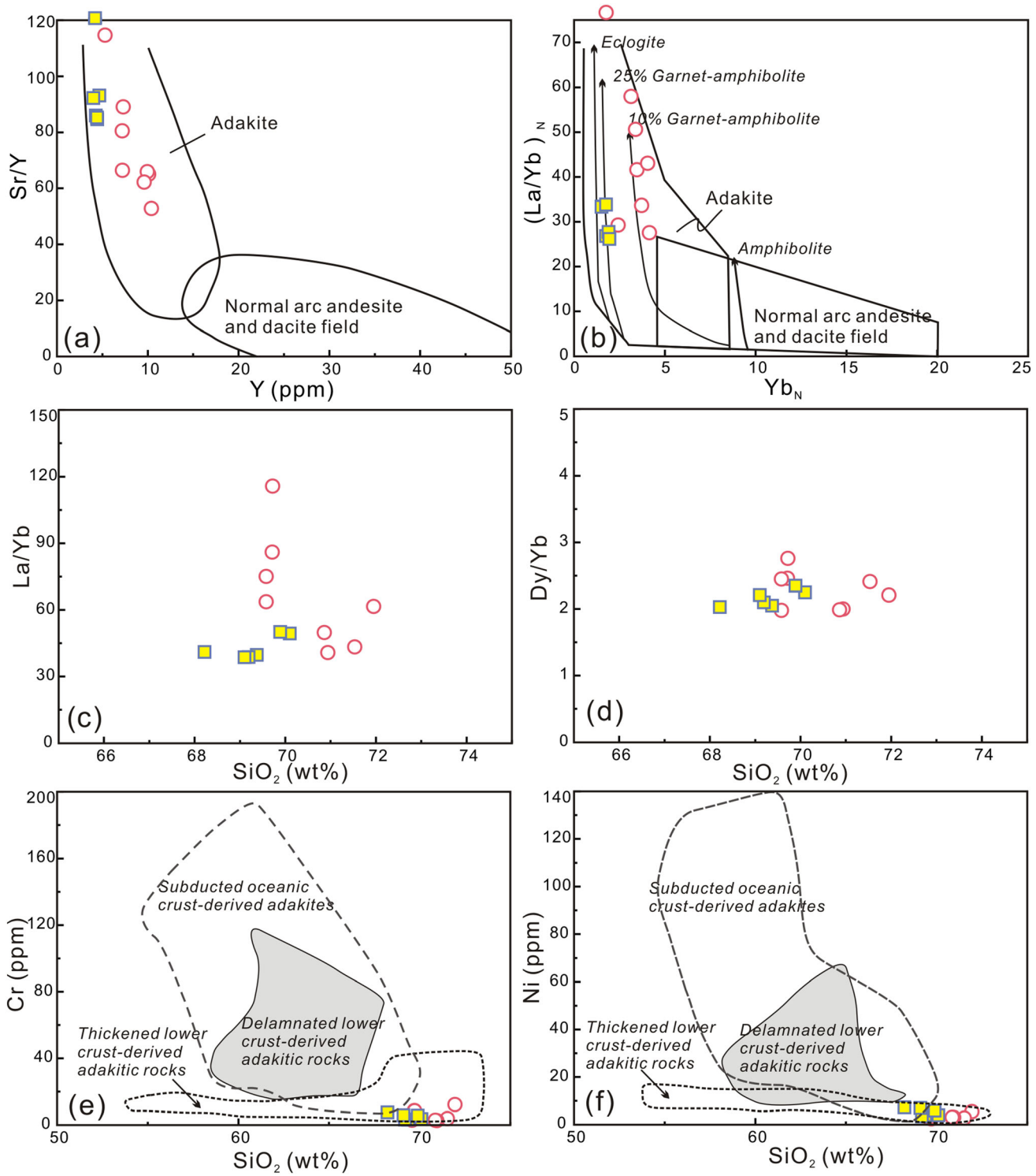

Fig. 6 **a** Sr/Y versus Y plot (after Defant and Drummond 1990); **b** $(La/Yb)_N$ versus Yb_N plot (after Drummond and Defant 1990); **c** La/Yb versus SiO_2 plot; **d** Dy/Yb versus SiO_2 plot; **e** Cr versus SiO_2 plot (after Wang et al. 2006); **f** Cr versus SiO_2 plot (after Wang et al. 2006). Symbols are the same as in Fig. 4

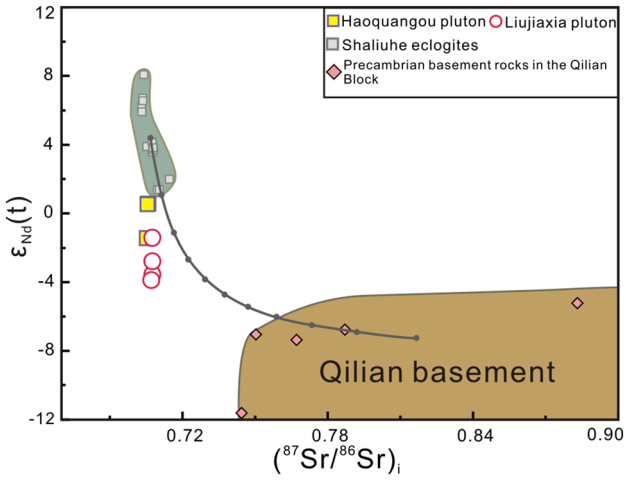

Fig. 7 Whole-rock $\varepsilon_{Nd}(t)$ versus $(^{87}Sr/^{86}Sr)_i$ diagram for the Liujiaxia and Haoquangou plutons (after Zhao et al. 2021)

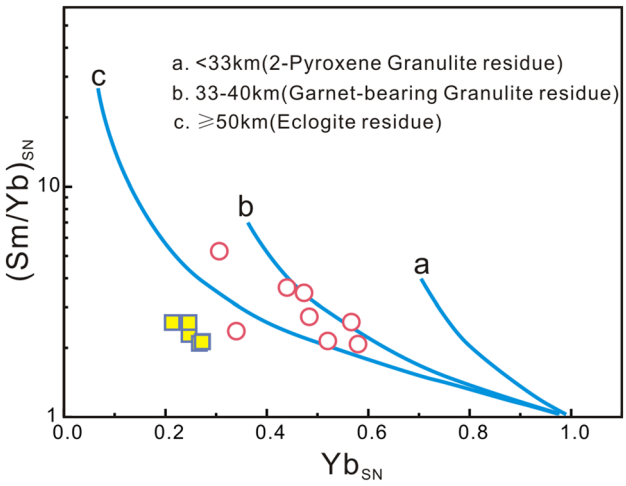

Fig. 8 $(Sm/Yb)_{SN}$ versus Yb_{SN} diagram for the adakitic Liujiaxia and Haoquangou granitoids (after Zhang et al. 2018); normalized values are average lower crust of Rudnick and Gao (2003). Symbols are the same as in Fig. 4

adakitic rocks (440–430 Ma) postdate the low-Mg ones (466–446 Ma) by 6 Myr (Zhang et al. 2019). The generation of the low-Mg and high-Mg adakitic rocks are considered to be related to partial melting of the thickened lower crust and anatexis of subsequent delaminated lower crust interacted with mantle peridotite, respectively (Tseng et al. 2009; Yu et al. 2015). Moreover, comprehensive magmatic, structural, and sedimentary evidence suggests that the final closure of the North Qilian Ocean between the Qilian Block and the Alxa Terrane occurred during the Late Ordovician (Song et al. 2013; Wang et al. 2019). Therefore, it is suggested that the Haoquangou adakitic rocks were generated in a post-collisional extensional regime due to lithospheric delamination (Fig. 9). Given their emplacement on the southern margin of the North Qilian orogenic belt and insignificant interaction between melt and mantle peridotite as revealed by low MgO content and Mg# values, the Haoquangou granidiorites were probably derived from partial melting of marginal residual thickened lower crust rather than the delaminated lower crust.

In contrast, based on the compilation of petrological evidence, Yang et al. (2020) and Zhao et al. (2022) concluded that the final closure of the South Qilian Ocean likely occurred at ca. 435 Ma. Moreover, Xia et al. (2016) proposed that the Qaidam Block started to collide at ca. 440 Ma, and was dragged beneath the Qilian Block by the downgoing oceanic lithosphere to depths of ~100–200 km at about 440–421 Ma. The 435–420 Ma granitoids in the Qilian Block generally show adakitic affinities and were contemporaneous with the UHP metamorphism in the NQ-UHPM belt, whereas those with ages of ca. 420–400 Ma are non-adakitic in compositions and occurred after the UHP metamorphism, revealing that their generations are closely related with subduction and exhumation of the continental crust, respectively (Yang et al. 2020; Zhao et al. 2022). The ca. 432 Ma Liujiaxia granites thus were the product of syn-collisional magmatism formed during the subduction of continental crust (Fig. 9).

Collectively, it is suggested that the Haoquangou pluton was formed during a post-collisional extensional setting, relating to the lithospheric delamination after the closure of the North Qilian Ocean, whereas the Liujiaxia pluton was generated in a compressive setting during a continental collision between the Qaidam and Qilian blocks.

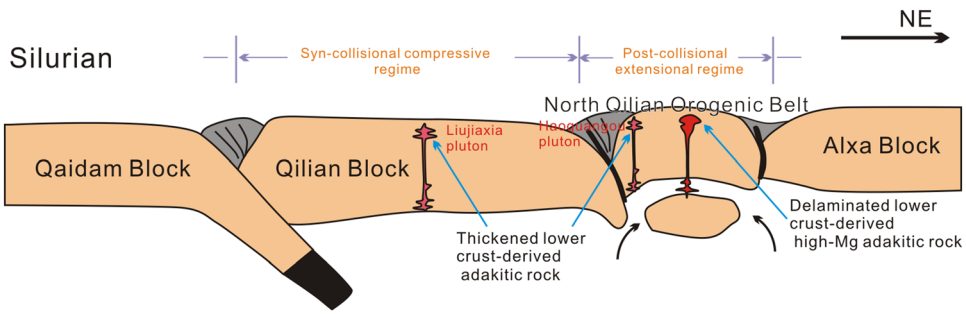

Fig. 9 Schematic illustration of the generation and emplacement of the Silurian Liujiaxia and Haoquangou plutons in the Qilian Orogenic Belt

7 Conclusions

(1) New LA–ICP–MS zircon U–Pb dating and whole-rock analysis results, combined with previous studies suggest that the Liujiaxia granites within the Qilian Block are high-K calc-alkaline, and were emplaced at ca. 432 Ma, while the Haoquangou granodiorites within the North Qilian orogenic belt are calc-alkaline, and were formed at ca. 423 Ma. Both of them are peraluminous in composition and show relatively depleted whole-rock Nd isotopic features, implying their derivation from a juvenile lower crust.

(2) The Liujiaxia and Haoquangou granitoids are characterized by low heavy REEs and Y concentrations and extremely high La/Yb and Sr/Y ratios, similar to adakites. Geochemical and whole-rock Sr–Nd isotopic data indicate that they were derived from the partial melting of thickened lower continental crust.

(3) The Haoquangou granodiorites within the North Qilian orogenic belt were generated in a post-collisional extensional regime related to the lithospheric delamination after the closure of the North Qilian Ocean between the Qilian and Alxa blocks. By comparison, the Liujiaxia granites were generated in a compressive setting during a continental collision between the Qaidam and Qilian blocks.

Acknowledgements This research was funded by Gansu Provincial Natural Science Foundation (Grant Numbers 21JR7RA503 and 22JR5RA819), the Fundamental Research Funds for the Central Universities (Grant lzujbky-2021-ct07), the Key Talent Project of Gansu Province (2022-Yangzhenxi) and the National Second Expedition to the Tibetan Plateau (2019QZKK0704).

Declarations

Conflict of interest The authors declare no conflict of interest.

References

Andersen T (2002) Correction of common lead in U–Pb analyses that do not report ^{204}Pb. Chem Geol 192:59–79

Atherton MP, Petford N (1993) Generation of sodium-rich magmas from newly underplated basaltic crust. Nature 362:144–146

Barbarin B (1999) A review of the relationships between granitoid types, their origins and their geodynamic environments. Lithos 46(3):605–626

Benito R, López-Ruiz J, Cebriá JM, Hertogen J, Doblas M, Oyarzun R, Demaiffe D (1999) Sr and O isotope constraints on source and crustal contamination in the high-K calc-alkaline and shoshonitic neogene volcanic rocks of SE Spain. Lithos 46(4):773–802

Black LP, Gulson BL (1978) The age of the mud tank carbonatite, strangways range, Northern territory. BMR J Aust Geol Geophys 3:227–232

Bonin B (2007) A-type granites and related rocks: evolution of a concept, problems and prospects. Lithos 97:1–29

Boynton WV (1984) Geochemistry of the rare Earth elements: meteorite studies. In: Henderson P (ed) Rare Earth Elements Geochemistry. Elservier, Amsterdam, pp 63–144

Castillo PR, Janney PE, Solidum RU (1999) Petrology and geochemistry of Camiguin Island, southern Philippines: insights to the source of adakites and other lavas in a complex arc setting. Contrib Mineral Petrol 134:33–51

Chappell BW, White AJR (1974) Two contrasting granite types. Pac Geol 8:173–174

Chen YX, Cui Y, Zhang LP, Fu SM, Wu K, Song SG, Sun WD, Xiao TF (2023) Sediment recycling and adakite petrogenesis: constraints from the late ordovician tonalite in the North Qilian suture zone. Chem Geol 624:121389

Chen B, Jahn BM, Suzuki K (2013) Petrological and Nd-Sr-Os isotopic constraints on the origin of high-Mg adakitic rocks from the North China Craton: tectonic implications. Geology 41:91–94

Chung SL, Liu D, Ji J, Chu MF, Lee HY, Wen DJ, Lo CH, Lee TY, Qian Q, Zhang Q (2003) Adakites from continental collision zones: melting of thickened lower crust beneath southern Tibet. Geology 31:1021–1024

Cui JW, Tian LM, Sun JY, Yang C (2019) Geochronology and geochemistry of early palaeozoic intrusive rocks in the Lajishan area of the eastern south Qilian Belt, Tibetan Plateau: implications for the tectonic evolution of south Qilian. Geol J 54:3404–3420

Dai HK, Zheng JP, Zhou X, Griffin WL (2017) Generation of continental adakitic rocks: crystallization modeling with variable bulk partition coefficients. Lithos 272–273:222–231

Dall'Agnol R, Frost CD, Rämö OT (2012) IGCP Project 510 A-type granites and related rocks through time: project vita, results, and contribution to granite research. Lithos 93:215–233

Defant MJ, Drummond MS (1990) Derivation of some modern arc magmas by melting of young subducted lithosphere. Nature 347:662–665

Eyal E, Litvinovsky B, John BM, Zanvilevich A, Katzir Y (2010) Origin and evolution of post–collisional magmatism: Coeval Neoproterozoic calc-alkaline and alkaline suites of the Sinai Peninsula. Chem Geol 269:153–179

Eyuboglu Y, Chung SL, Santosh M, Dudas FO, Akaryal E (2011) Transition from shoshonitic to adakitic magmatism in the eastern Pontides, NE Turkey: implications for slab window melting. Gondwana Res 19(2):413–429

Gao JF, Lu JJ, Lin YP, Pu W (2003) Analysis of trace elements in rock samples using HR-ICPMS. J Nanjing Univ (Nat Sci) 39:844–850 (in Chinese with English abstract)

Ge XY, Li XH, Chen ZG, Li WP (2002) Geochemistry and petrogenesis of Jurassic high Sr/low Y granitoids in eastern China: constrains on crustal thickness. Chin Sci Bull 47(11):962–968

Hu J, Jiang SY, Zhao HX, Shao Y, Zhang ZZ, Xiao E, Wang YF, Dai BZ, Li HY (2012) Geochemistry and petrogenesis of the Huashan granites and their implications for the mesozoic tectonic settings in the Xiaoqinling gold mineralization belt, NW China. J Asian Earth Sci 56:276–289

Huang H, Niu Y, Nowell G, Zhao Z, Yu X, Mo X (2015) The nature and history of the Qilian Block in the context of the development of the greater Tibetan Plateau. Gondwana Res 28(1):209–224

Irvine TN, Baragar WRA (1971) A guide to the chemical classification of the common volcanic rocks. Can J Earth Sci 8:523–548

Li SM, Zhu DC, Wang Q, Zhao Z, Zhang LL, Liu SA (2016) Slab-derived adakites and subslab asthenosphere-derived OIB-type rocks at 156 ± 2 Ma from the north of Gerze, central Tibet: records of the bangong–nujiang oceanic ridge subduction during the late jurassic. Lithos 262:456–469

Li S, Zhao S, Liu X, Cao H, Yu S, Li X (2018) Closure of the Proto-Tethys ocean and Early Paleozoic amalgamation of microcontinental blocks in east Asia. Earth Sci Rev 186:37–75

Liégeois JP (1998) Preface–Some words on the post-collisional magmatism. Lithos 45:15–17

Litvinovsky BA, Tsygankov AA, Jahn BM, Katzir Y, Be'eri-Shlevin Y (2011) Origin and evolution of overlapping calc-alkaline and alkaline magmas: the late palaeozoic post-collisional igneous province of Transbaikalia (Russia). Lithos 125:845–874

Ma Q, Xu YG, Zheng JP, Griffin WL, Hong LB, Ma L (2016) Coexisting Early Cretaceous high-Mg andesites and adakitic rocks in the North China Craton: the role of water in intraplate magmatism and cratonic destruction. J Petrol 57(7):1279–1308

Maniar PD, Piccoli PM (1989) Tectonic discrimination of granitoids. Geol Soc Am Bull 101:635–643

Martin H (1999) The adakitic magmas: modern analogues of archaean granitoids. Lithos 46(3):411–429

McDonough WF, Sun SS (1995) The composition of the Earth. Chem Geol 120:223–253

Middlemost EAK (1994) Naming materials in the magma/igneous rock system. Earth Sci Rev 37:215–224

Mo XX, Niu YL, Dong GC, Zhao ZD, Hou ZQ, Su Z, Ke S (2008) Contribution of syncollisional felsic magmatism to continental crust growth: a case study of the Paleogene Linzizong volcanic succession in southern Tibet. Chem Geol 250:49–67

Moyen JF (2009) High Sr/Y and La/Yb ratios: the meaning of the adakitic signature. Lithos 112:556–574

Nagel TJ, Hoffmann JE, Münker C (2012) Generation of Eoarchean tonalite-trondhjemite-granodiorite series from thickened mafic arc crust. Geology 40(4):375–378

Niu YL, Zhao ZD, Zhu DC, Mo XX (2013) Continental collision zones are primary sites for net continental crust growth—A testable hypothesis. Earth Sci Rev 127:96–110

Peccerillo A, Taylor DR (1976) Geochemistry of Eocene calc-alkaline volcanic rocks from the Kaitamonu area, Northern Turkey. Contrib Mineral Petrol 58:63–91

Qian Q, Hermann J (2013) Partial melting of lower crust at 10–15 kbar: constraints on adakite and TTG formation. Contrib Mineral Petrol 165:1195–1224

Rapp RP, Shimizu N, Norman MD, Applegate GS (1999) Reaction between slab-derived melts and peridotite in the mantle wedge: experimental constraints at 3.8 GPa. Chem Geol 160:335–356

Rudnick RL, Gao S (2003) Composition of the continental crust. Crust Treatise Geochem 3:1–64

Sisson T, Ratajeski K, Hankins W, Glazner A (2005) Voluminous granitic magmas from common basaltic sources. Contrib Mineral Petrol 148:635–661

Song SG, Niu YL, Su L, Xia XH (2013) Tectonics of the North Qilian orogen, NW China. Gondwana Res 23(4):1378–1401

Song SG, Niu YL, Su L, Zhang C, Zhang LF (2014) Continental orogenesis from ocean subduction, continent collision/subduction, to orogen collapse, and orogen recycling: the example of the North Qaidam UHPM belt, NW China. Earth Sci Rev 129:59–84

Tseng CY, Yang HJ, Yang HY, Liu D, Wu C, Cheng CK, Chen CH, Ker CM (2009) Continuity of the North Qilian and North Qinling orogenic belts, central orogenic system of China: evidence from newly discovered Paleozoic adakitic rocks. Gondwana Res 16:285–293

Tung KA, Yang HY, Yang HJ, Smith A, Liu D, Zhang J (2016) Magma sources and petrogenesis of the Early-Middle Paleozoic backarc granitoids from the central part of the Qilian Block, NW china. Gondwana Res 38:197–219

Wang Q, Xu JF, Jian P, Bao ZW, Zhao ZH, Li CF, Xiong XL, Ma JL (2006) Petrogenesis of adakitic porphyries in an extensional tectonic setting, Dexing, South China: implications for the genesis of porphyry copper mineralization. J Petrol 47(1):119–144

Wang KX, Yu CD, Yan J, Liu XD, Liu WH, Pan JY (2019) Petrogenesis of early silurian granitoids in the Longshoushan area and their implications for the extensional environment of the North Qilian Orogenic Belt, China. Lithos 342–343:152–174

Xia LQ, Li XM, Yu JY, Wang GQ (2016) Mid–Late Neoproterozoic to Early Paleozoic volcanism and tectonic evolution of the Qilian mountain. Geol China 43(4):1087–1138 (**in Chinese with English abstract**)

Xie YH, Li XW, Mo XX, Dong GC, Sun YQ, Shan W (2023) The effects of the source composition on the origin of orthopyroxene-bearing adakitic granitoid in West Qinling, Central China. Geosci Front 14:101554

Yang XQ, Zhang ZH, Jiang ZS, Duan SG (2018) Geochronology, petrogenesis and tectonic significance of Huashugou granit-oids in North Qilian, NW China. Lithos 314–315:497–505

Yang H, Zhang HF, Xiao WJ, Luo BJ, Gao Z, Tao L, Zhang LQ, Guo L (2020a) Petrogenesis of Early Paleozoic high Sr/Y intrusive rocks from the North Qilian orogen: implication for diachronous continental collision. Lithosphere 12:53–73

Yang S, Su L, Song SG, Allen MB, Feng D, Wang M, Wang C, Zhang H (2020) Melting of subducted continental crust during collision and exhumation: insights from granitic rocks from the North Qaidam UHP metamorphic belt. NW China Lithos 378–379:105794

Yang H, Zhang HF, Xiao WJ, Tao L, Gao Z, Luo BJ, Zhang LQ (2021) Multiple Early Paleozoic granitoids from the southeastern Qilian orogen, NW China: magma responses to slab roll-back and break-off. Lithos 380–381:105910

Yao JL, Cawood PA, Zhao GC, Han YG, Xia XP, Liu Q, Wang P (2021) Mariana type ophiolites constrain establishment of modern plate tectonic regime during Gondwana assembly. Nat Commun 12:4189

Yu S, Zhang J, Qin H, Sun D, Zhao X, Cong F, Li Y (2015) Petrogenesis of the Early Paleozoic low-Mg and high-Mg adakitic rocks in the North Qilian Orogenic belt, NW China: implications for transition from crustal thickening to extension thinning. J Asian Earth Sci 107:122–139

Yu SY, Peng YB, Zhang JX, Li SZ, Santosh M, Li YS (2021) Tectono-thermal evolution of the Qilian orogenic system: tracing the subduction, accretion and closure of the Proto-Tethys Ocean. Earth Sci Rev 215:103547

Yuan H, Gao S, Dai M, Zong C, Günther D, Fontaine GH, Liu X, Diwu C (2008) Simultaneous determinations of U–Pb age, hf isotopes and trace element compositions of zircon by excimer laser-ablation quadrupole and multiplecollector ICP–MS. Chem Geol 247:100–118

Zhang L, Zhang H, Zhang S, Xiong Z, Luo B, Yang H, Pan FB, Zhou XC, Xu WC, Guo L (2017) Lithospheric delamination in post-collisional setting: evidence from intrusive magmatism from the North Qilian orogen to southern margin of the Alxa block, NW China. Lithos 288–289:20–34

Zhang H, Li SQ, Fang BW, He JF, Xue YY, Siebel W, Chen FK (2018) Zircon U–Pb ages and geochemistry of migmatites and granites in the foping dome: evidence for Late Triassic crustal evolution in South Qinling, China. Lithos 296–299:129–141

Zhang HR, Zhao JL, Yu HY (2019) Petrogenesis and tectonic implications of the Laohushan Quartz Diorite from the Eastern part of North Qilian Orogen, NW China. Geol J China Univ 25(5):641–653

Zhao GB, Yang HQ, Ren HN, Jia J, Wang YH, Li JC, Zhou H (2013) LA-ICP-MS zircon U–Pb ages of Heishishan granite bodies in north Qilian and their geological significance. Geol Bull China 32(10):1575–1583

Zhao JL, Qiu JS, Liu L, Wang RQ (2016) The Late Cretaceous I- and A-type granite association of southeast China: implications for the origin and evolution of post-collisional extensional magmatism. Lithos 240–243:16–33

Zhao JL, Wu B, Zhang X, Chen WF, Ma XX (2021) Petrogenesis of Early Paleozoic adakitic granitoids in the eastern Qilian Block, northwest China: implications for the South Qilian Ocean subduction. Mineral Petrol 115:687–708

Zhao JL, Zhang X, Wang JR, Tang QY, Zhou WN, Ma XX (2022) Syn-orogenic tectonomagmatic evolution of the Qilian Orogen: insights from the Lumanshan gabbro–granite association in the Qilian Block, Northwest China. Lithos 434–435:106922